Fabrication of Ni-Ti-O nanotube arrays by anodization of NiTi alloy and their potential applications

Ruiqiang Hang[1], Yanlian Liu[1], Lingzhou Zhao[2], Ang Gao[3], Long Bai[1], Xiaobo Huang[1], Xiangyu Zhang[1], Bin Tang[1] & Paul K. Chu[3]

[1]Research Institute of Surface Engineering, Taiyuan University of Technology No. 79 Yingze West Road, Taiyuan 030024, China, [2]State Key Laboratory of Military Stomatology, Department of Periodontology, School of Stomatology, The Fourth Military Medical University No. 145 West Changle Road, Xi'an 710032, China, [3]Department of Physics and Materials Science, City University of Hong Kong Tat Chee Avenue, Kowloon, Hong Kong, China.

Nickel-titanium-oxide (Ni-Ti-O) nanotube arrays (NTAs) prepared on nearly equiatomic NiTi alloy shall have broad application potential such as for energy storage and biomedicine, but their precise structure control is a great challenge because of the high content of alloying element of Ni, a non-valve metal that cannot form a compact electronic insulating passive layer when anodized. In the present work, we systemically investigated the influence of various anodization parameters on the formation and structure of Ni-Ti-O NTAs and their potential applications. Our results show that well controlled NTAs can be fabricated during relatively wide ranges of the anodization voltage (5–90 V), electrolyte temperature (10–50°C) and electrolyte NH_4F content (0.025–0.8 wt%) but within a narrow window of the electrolyte H_2O content (0.0–1.0 vol%). Through modulating these parameters, the Ni-Ti-O NTAs with different diameter (15–70 nm) and length (45–1320 nm) can be produced in a controlled manner. Regarding potential applications, the Ni-Ti-O NTAs may be used as electrodes for electrochemical energy storage and non-enzymic glucose detection, and may constitute nanoscaled biofunctional coating to improve the biological performance of NiTi based biomedical implants.

N anotube arrays (NTAs) prepared by electrochemical anodization have captured tremendous interest in energy[1–3], environment[3–5], biomedicine[3,6–9], as well as many other fields. The growth of NTAs during anodization is mainly ascribed to the presence of the appropriate amount of F⁻ ion and the underlying mechanism has been summarized in recent works[3,10]. Based on the same principle, NTAs have been fabricated on a variety of valve metals[3,10], including titanium (Ti), zirconium (Zr), hafnium (Hf), tantalum (Ta), niobium (Nb), vanadium (V), and so on. The most widely investigated one is TiO_2 NTAs because of the excellent semiconducting property and biocompatibility of TiO_2[3].

In order to improve the performance of TiO_2 NTAs and widen their applications, elemental doping is a feasible approach. In this respect, a straightforward and efficient way is an anodization treatment of Ti-X alloys where X is the expected dopant. Doped TiO_2 NTAs have hitherto been produced by anodization of various alloys such as TiAu, TiPt, TiZr, TiW, TiMo, TiNb, TiAl, TiCu, TiAg, TiFe, TiMn, TiRu, TiHf, TiV, and TiNi to attain specific functions[3,11–19]. For example, Au doped TiO_2 NTAs have been proven to be a highly efficient photocatalyst to produce H_2 from splitting water[11]. Ag doped TiO_2 NTAs show long-term antibacterial ability and simultaneously good biocompatibility thus being potential biomedical implant coatings[13]. The anodization behavior of Ti-X alloys depends closely on the alloying element X. For instance, TiRu alloy with small concentrations of Ru (a typical non-valve element that cannot form a compact electronic insulating passive layer when anodized) of less than 5 at% allows the formation of well-defined NTAs[16], whereas regular NTAs can be formed on the TiZr alloy in a wider concentration range of Zr (a typical valve element) of up to 50 wt%[20]. NTAs appear to be relatively easy to form on Ti alloys with valve alloying elements in a wide content range of the alloying elements, but much harder on Ti alloys with non-valve alloying elements confined to only a small concentration of the alloying element. Fabrication of well-defined NTAs with a large content of non-valve metals is thus challenging.

It is of interest to study the anodization behavior of nearly equiatomic NiTi alloy (50.8at% Ni) in terms of the following aspects. Firstly, NiO and NiO/TiO_2 composites have many unique properties that can be exploited in electrochemical energy storage, photocatalysis, biosensors, resistance switching, and electrochromic fields[19,21–24].

In most of these applications, usually a large surface area per unit mass is needed to achieve a high efficiency. Ni doped NTAs are expected to cater to this requirement. Secondly, NiTi alloys have been widely used in biomedical implants due to its notable shape memory and super-elastic properties, but further improvement in terms of bioactivity is needed to achieve more satisfactory tissue integration. NTAs formed by anodization may constitute a nano-functional coating on NiTi based implants to improve the biological performance[25,26]. Thirdly, the work will provide insights into the anodization of Ti alloys with a large content of non-valve elements. Since the report on anodization of NiTi alloy to form Ni-Ti-O NTAs by Frank and co-authors[19], there have been very limited publications regarding this topic and in particular, precise structural control of Ni-Ti-O NTAs is quite difficult due to the large Ni content[26–28]. Herein, the influence of various anodization parameters such as anodization duration and voltage as well as the composition and temperature of electrolyte on the formation and structure of the Ni-Ti-O NTAs is investigated systematically. The feasibility of producing well-controlled Ni-Ti-O NTAs on NiTi alloy by modulating these parameters is demonstrated and their potential applications to the energy storage as well as environmental and biomedical fields are explored.

Methods

The NiTi alloy (50.8 at % Ni) was cut into small sheets (7.5 mm × 7.5 mm × 2 mm) and polished to a mirror finish. A copper wire of 100 mm long was attached to the non-working face of the NiTi sheet with the copper conductive tapes, which was then sealed with the silicone rubber. The distance between the working electrode and the counterpart of Pt foil (10 mm × 10 mm × 0.2 mm) was set at 20 mm. Each sample was anodized in the electrolyte of 100 ml with a DC power supply. The electrochemical cell was covered with a PVC film during anodization to prevent the dissolution of H_2O from atmosphere to the electrolyte. The temperature of the electrolyte was controlled by a thermostatic bath. After anodization, all samples were washed with distilled water for 30 s immediately. To investigate the effects of the anodization voltage, the samples were anodized at 30°C and 5 V, 10 V, 15 V, 20 V, 25 V, 30 V, 40 V, 60 V, and 90 V in ethylene glycol (Sinopharm Chemical Reagent, China) containing 0.2 wt% NH_4F (Sinopharm Chemical Reagent, China) and 1.0 vol% H_2O. To investigate the influence of the anodization temperature, the samples were anodized at 25 V and 10°C, 20°C, 30°C, 40°C, and 50°C in ethylene glycol supplemented with 0.2 wt% NH_4F and 0.5 vol% H_2O for 1 h and to investigate the effects of the anodization time, the samples were anodized at 30°C and 25 V in ethylene glycol containing 0.2 wt% NH_4F and 1.0 vol% H_2O for 5 min, 15 min, 30 min, 60 min, and 120 min. To study the influence of the H_2O concentration, the samples were anodized at 30°C and 25 V in ethylene glycol with 0.2 wt% NH_4F and 0.0 vol%, 0.25 vol%, 0.5 vol%, 1.0 vol%, 1.5 vol%, and 2.0 vol% H_2O for 1 h and to investigate the influence of the F^- content, the samples were anodized at 30°C and 25 V in ethylene glycol supplemented with 1.0 vol% H_2O and 0.025 wt%, 0.05 wt%, 0.1 wt%, 0.2 wt%, 0.4 wt%, 0.8 wt%, and 1.0 wt% NH_4F for 1 h.

Field-emission scanning electron microscopy (FE-SEM, JSM-6700F, JEOL) and high resolution transmission electron microscopy (HR-TEM, JEM-2100F, JEOL) were conducted to examine the morphology and microstructure of the anodized samples. The elemental composition and chemical states were determined by X-ray photoelectron spectroscopy (XPS, K-Alpha, Thermo) employing monochromatic Al K_α radiation (6 mA, 12 kV, and 1486.68 eV). The three-dimensional morphology of the corrosion micropits was assessed by laser scanning confocal microscopy (LSCM, OLS4100, OLYMPUS) and an electrochemical workstation (CS350, CorrTest) was employed to acquire the current-time curves during anodization.

The electrochemical capacitance performance of the NTAs is assessed. The electrode composed of NTAs on the NiTi alloy with an exposed area of 0.5 cm² was used in the electrochemical tests conducted in a 1 M KOH solution at room temperature on the electrochemical workstation (CS350, CorrTest). A three-electrode system with SCE as the reference electrode and Pt foil as the counter electrode was used. The electrochemical behavior was characterized by CV and GCD tests. The CV tests were performed in the potential range between 0 and 0.5 V (vs. SCE) at scanning rates of 5, 20, 50, 100, 200, 500, and 1000 mV/s and the GCD curves were obtained between 0 and 0.5 V (vs. SCE) at a current density of 0.4 mA/cm². The electrochemical impedance spectroscopy (EIS) measurement was conducted at open circuit potential (OCP) with a sinusoidal perturbation potential of 10 mV within a frequency range of 100 kHz to 1 mHz.

The glucose sensing ability of the Ni-Ti-O NTAs was measured by cyclic voltammetry on the electrochemical workstation at room temperature. NaOH solutions
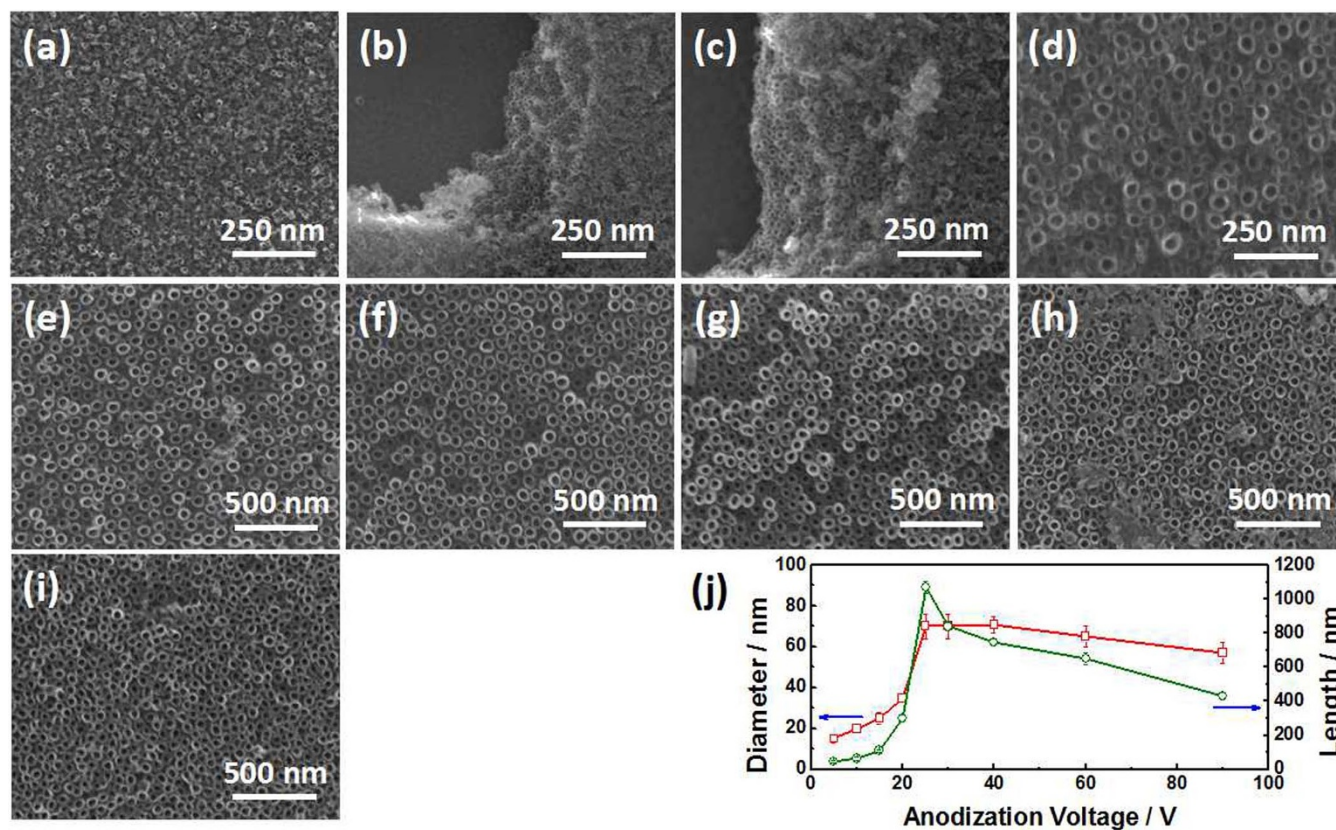

Figure 1 | Surface FE-SEM images of the Ni-Ti-O NTAs formed in ethylene glycol containing 0.2 wt% NH_4F and 1.0 vol% H_2O at 30°C at different anodization voltages. (a) 5 V, (b) 10 V, (c) 15 V, (d) 20 V, (e) 25 V, (f) 30 V, (g) 40 V, (h) 60 V, and (i) 90 V. The anodization durations at different voltages are 12, 6, 6, 4, 1, 0.5, 0.5, 0.25, and 0.25 h, respectively, to reach their balanced (maximum) nanotube length. Variation in the diameter and length of the NTs as a function of anodization voltage (j).

(0.1 M) of 50 ml containing different concentrations of glucose were used as the electrolyte and the Pt foil (10 mm × 10 mm × 0.2 mm) was used as the counterpart. All potentials were referenced to the Ag/AgCl reference electrode in the measurement. The mirror polished NiTi alloy was also used as a comparison. The electrodes were activated in the NaOH solution (0.1 M) at a scanning rate of 50 mV/s for 100 cycles before the electrochemical tests.

In the biological experiments, the cell viability was evaluated by live/dead staining. After autoclave sterilization, each sample was placed on one of the wells on a 24-well cell culture plate, seeded with MC3T3-E1 subclone 14 pre-osteoblastic cells at a density of 2.0×10^4 cells/cm^2, and cultured in α-MEM (Gibco) supplemented with 10% calf bovine serum (CBS), 100 units/ml penicillin, and 100 μg/ml streptomycin in a humidified atmosphere of 5% CO_2 at 37°C. After culturing for 1, 3, and 7 days, the samples were rinsed with PBS, stained with the LIVE/DEAD® viability/cytocoxicity kit for mammalian cells (Invitrogen) for 1 h at 37°C, rinsed with PBS again, and observed by fluorescence microscopy (BM-20AYC, BM).

The photocatalytic activity of the samples was evaluated using a 300 W Xenon lamp. The preparation parameters of the Ni-Ti-O NTAs are the same as those in the electrochemical capacitance experiments. The TiO$_2$ NTAs with the same morphology as Ni-Ti-O NTAs were used as the control. Each sample with an apparent area of 2 cm^2 was incubated in 2 ml of a solution of methylene blue (1.2×10^{-5} M) in a glass cuvette for 1 h before irradiation to establish the adsorption-desorption equilibrium on the NTAs. The decomposition rate of the dye was evaluated by measuring the absorbance of the solutions periodically every 10 min on a UV/Vis spectrophotometer (UV-1100, Mapada).

Results and Disscusion

The effect of the anodization voltage on the structure of Ni-Ti-O NTAs is shown in Figure 1. The samples are fabricated by anodization in an ethylene glycol solution containing 0.2 wt% NH$_4$F and 1.0 vol% H$_2$O at 30°C. At a low voltage of 5 V, nanotubes (NTs) with a small diameter of about 15 nm are observed. Increasing the voltage from 10 to 25 V results in a linear increase in the NT diameter to 70 nm at 25 V. The NT diameter remains the same in the voltage range of 25-40 V and further voltage increase leads to a slight decrease in the NT diameter to 65 and 60 nm at 60 and 90 V, respectively. The variation in the NT length versus anodization volt-age shows a similar trend as that of the diameter, with the largest length of about 1100 nm generated at 25 V. When the voltage exceeds 25 V, evenly distributed micropits occur (Figure S1f-i). The entire surface of micropits is covered by NTAs, but the diameter and length are smaller than those outside the micropits (Figure S2). The elemental composition inside and outside the micropits shows no obvious difference as evidenced by Energy dispersive spectroscopy (EDS) elemental mapping (Figure S3). The variation of current during anodization is similar to that of pure Ti, but its steady-state value is higher. When the voltage exceeds 25 V, current fluctuation in the steady-state phase during the anodization process can be observed (Figure S4a). It is generally accepted that a larger voltage leads to increased NT diameter and length in anodization of pure Ti[29], but in case of NiTi alloy, this rule no longer applies when the voltage exceeds 25 V. The deviation may be explained by runaway anodization at an elevated voltage, namely current self-amplification resulting from the resistance heating effect. The resistance heating effect elevates the temperature, which on the one hand accelerates oxide dissolution reducing the NT diameter and length, but on the other hand promotes the formation of electrochemical active sites on the sample surface causing local thinning, breakdown of the oxide film, and formation of micropits[30]. The micropits act as short-circuit channels to increase the current further heating the sample. After initiation, the micropits will proliferate in both depth and width (Figure S5). At the same time, hydrolysis of metal cations such as Ti^{4+} and Ni^{2+} enriched in the micropits reduces the local pH thus accelerating oxide dissolution and decreasing the NT length and diameter in the micropits.

The influence of the electrolyte temperature on the structure of NTAs is displayed in Figure 2. The samples are anodized at 25 V in ethylene glycol with 0.2 wt% NH$_4$F and 0.5 vol% H$_2$O for 1 h. As the
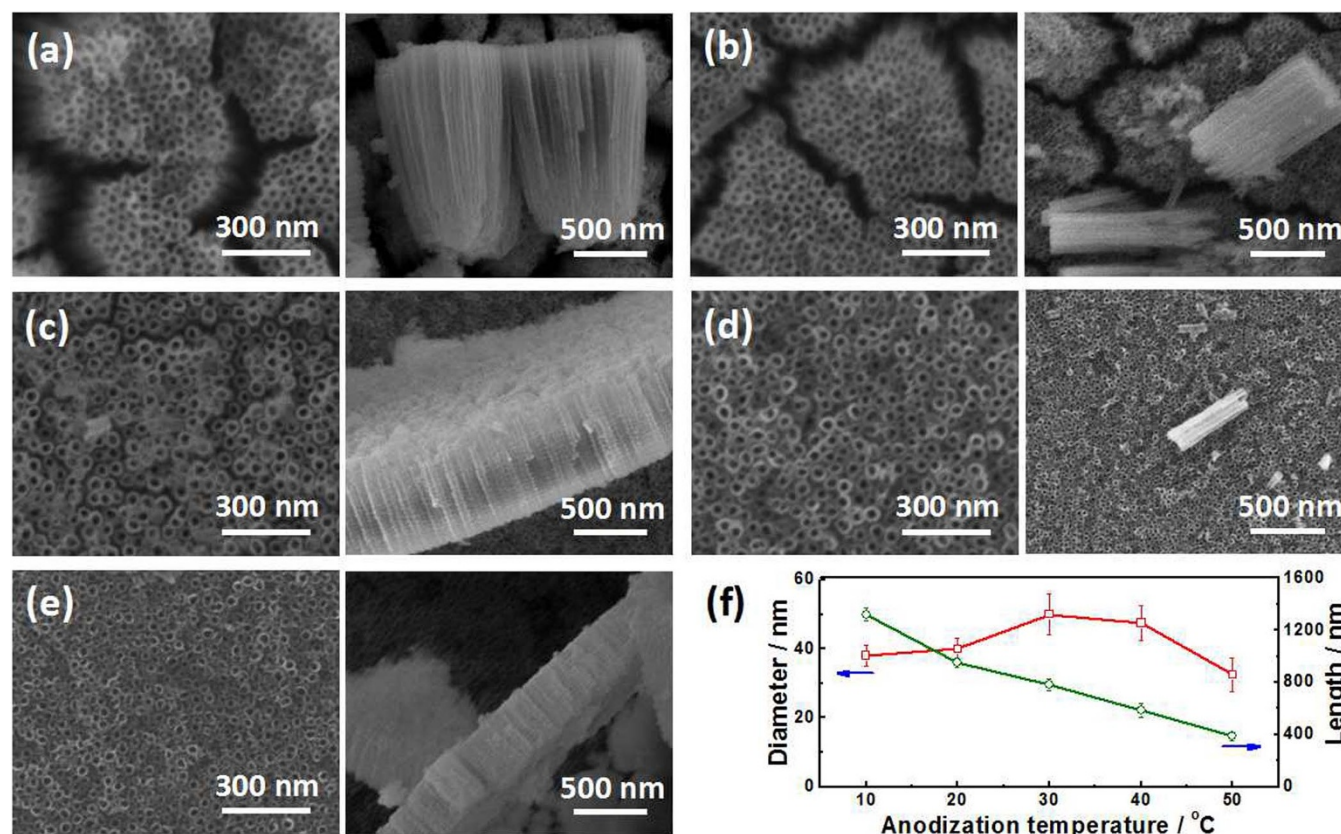

Figure 2 | Surface and cross-sectional FE-SEM images of Ni-Ti-O NTAs formed in ethylene glycol with 0.2 wt% NH$_4$F and 0.5 vol% H$_2$O at 25 V at different anodization temperature. (a) 10°C, (b) 20°C, (c) 30°C, (d) 40°C, and (e) 50°C for 1 h. Variation in the diameter and length of the NTs as a function of anodization temperature (f).
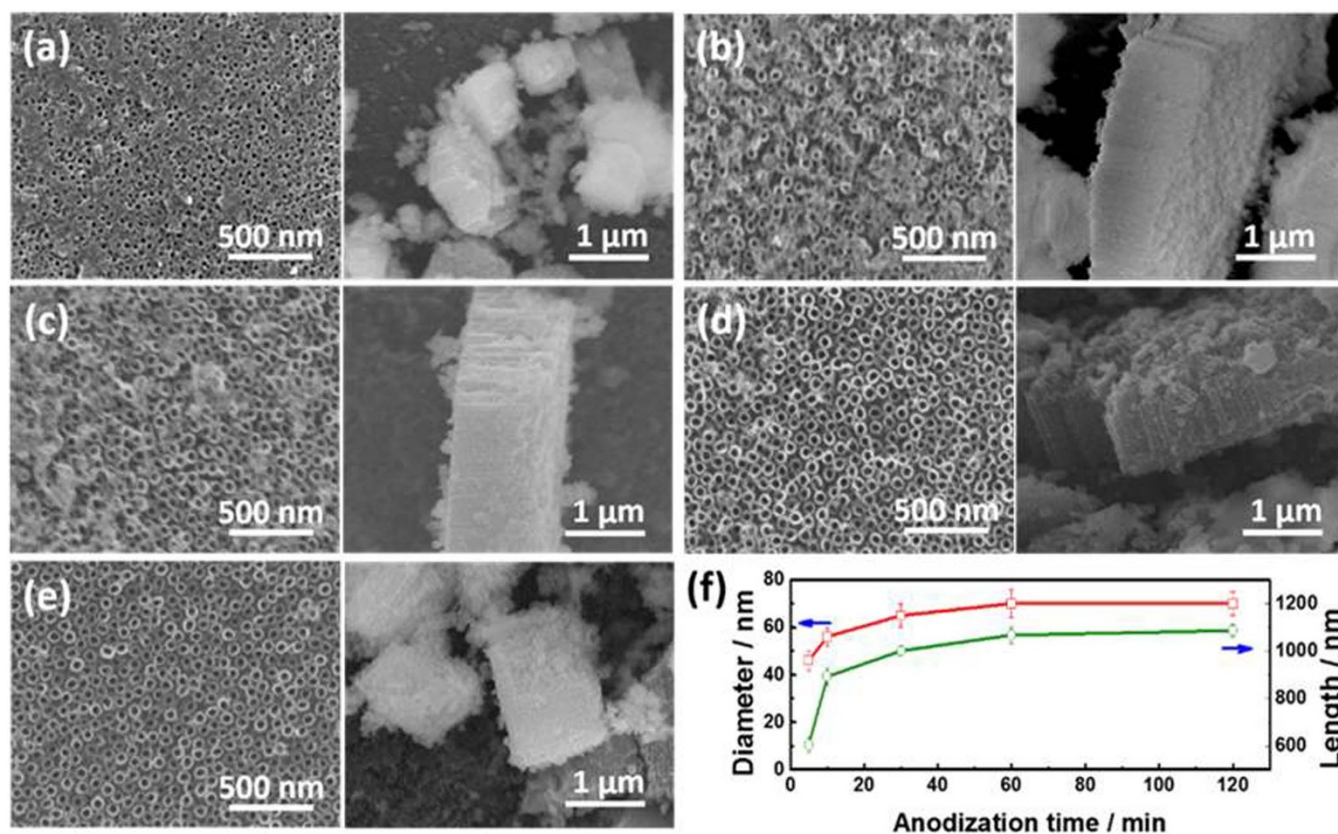
Figure 3 | Surface and cross-sectional FE-SEM images of the Ni-Ti-O NTAs formed in ethylene glycol with 0.2 wt% NH$_4$F and 1.0 vol% H$_2$O at 25 V and 30°C for different anodization time. (a) 5 min, (b) 15 min, (c) 30 min, (d) 60 min, and (e) 120 min. Variation in the diameter and length of the NTs as a function of anodization time (f).

electrolyte temperature goes up, the NT diameter increases initially and then decreases when the temperature is over 30°C, but the variation is not too large (38–50 nm). The NT length decreases linelly from 1,320 to 386 nm when the electrolyte temperature is raised from 10 to 50°C. A higher temperature reduces the electrolyte viscosity that can induce two opposite effects during electrochemical anodization. Firstly, it increases the mobility of H$_2$O and F$^-$ ions in the electrolyte to accelerate NT growth, as evidenced by the increasing current with electrolyte temperature illustrated in Figure S4b and secondly, it accelerates the chemical etching rate to shorten the NTs. During anodization of pure Ti, a linear increase in the tube length is observed as the anodization temperature is raised[29], providing evidence of the domination of the first effect. However, anodization of NiTi alloy here exhibits a completely opposite tendency, implying that chemical dissolution of nickel oxide may be more sensitive to the temperature rise and the second effect is dominant in the NiTi alloy anodization process. It can be concluded that in order to fabricate long Ni-Ti-O NTAs, a low electrolyte temperature is required. Another phenomenon is that the Ni-Ti-O NTAs formed at a low electrolyte temperature form bundles separated by cracks (Figure 2 and Figure S6). With increasing NT length, their mechanical strength may not withstand the capillary force thus resulting in clustering[3]. In addition, irregular macroscopic corrosion grooves are observed after anodization at a relatively high temperature (Figure S7) and this is consistent with the current fluctuation in the steady stage on the current-time curves (Figure S4b), which may be related to runaway anodization.

The effects of the anodization time on the NTA structure are investigated. Anodization is conducted at 30°C and 25 V in an ethylene glycol solution containing 0.2 wt% NH$_4$F and 1.0 vol% H$_2$O. As shown in Figure 3, the NT length increases rapidly initially and slows down gradually afterwards. After anodization for 60 min, the NT

length is nearly steady at about 1,100 nm. It is well known that the final NT length is determined by the anodization duration as well as growth and dissolution rates of the oxide. Our results indicate that after anodization for 60 min, a balance is established between the growth rate on the bottom of NTs and dissolution rate on the top. The anodization time influences the NT diameter in a way similarly to the NT length. With increasing anodization duration and NT length, the transport of F$^-$ to the electrolyte/oxide interface becomes more difficult. Hence, etching of the NT by F$^-$ slows and consequently, the bottom oxide thickness and NT diameter increase[3]. After anodization of 60 min, the tube length does not increase further because the availability of F$^-$ at the electrolyte/oxide interface and etching rate of F$^-$ ion on the bottom of the NTs become constant thereby leading to a steady state with respect to the NT diameter. Another phenomenon that should be noted is the irregular surface layer. Generally, in the initial stage of anodization, an irregular surface layer forms and it is gradually removed as anodization proceeds. Our results indicate that an anodization duration of 60 min is required to remove this layer in order to expose the underlying nanotubular structure.

The composition of the anodization electrolyte is another important parameter determining the NTA structure. The effects of the H$_2$O content in the electrolyte are shown in Figure 4. The samples are anodized at 30°C and 25 V in ethylene glycol with 0.2 wt% NH$_4$F but different H$_2$O concentrations for 1 h. NTAs are observed for H$_2$O contents between 0.0 and 1.0 vol% in the electrolyte. Excess H$_2$O leads to an irregular porous structure (Figures 4e and f) because of fast oxide dissolution. When the H$_2$O content is 0 vol%, a thick irregular surface layer can be observed on the NTAs. As the H$_2$O content is increased, this irregular surface layer dissolves gradually and finally disappears at a cocentration of 0.5 vol%. In the range of 0.0–1.0 vol%, the NT diameter and length increase linearly with the
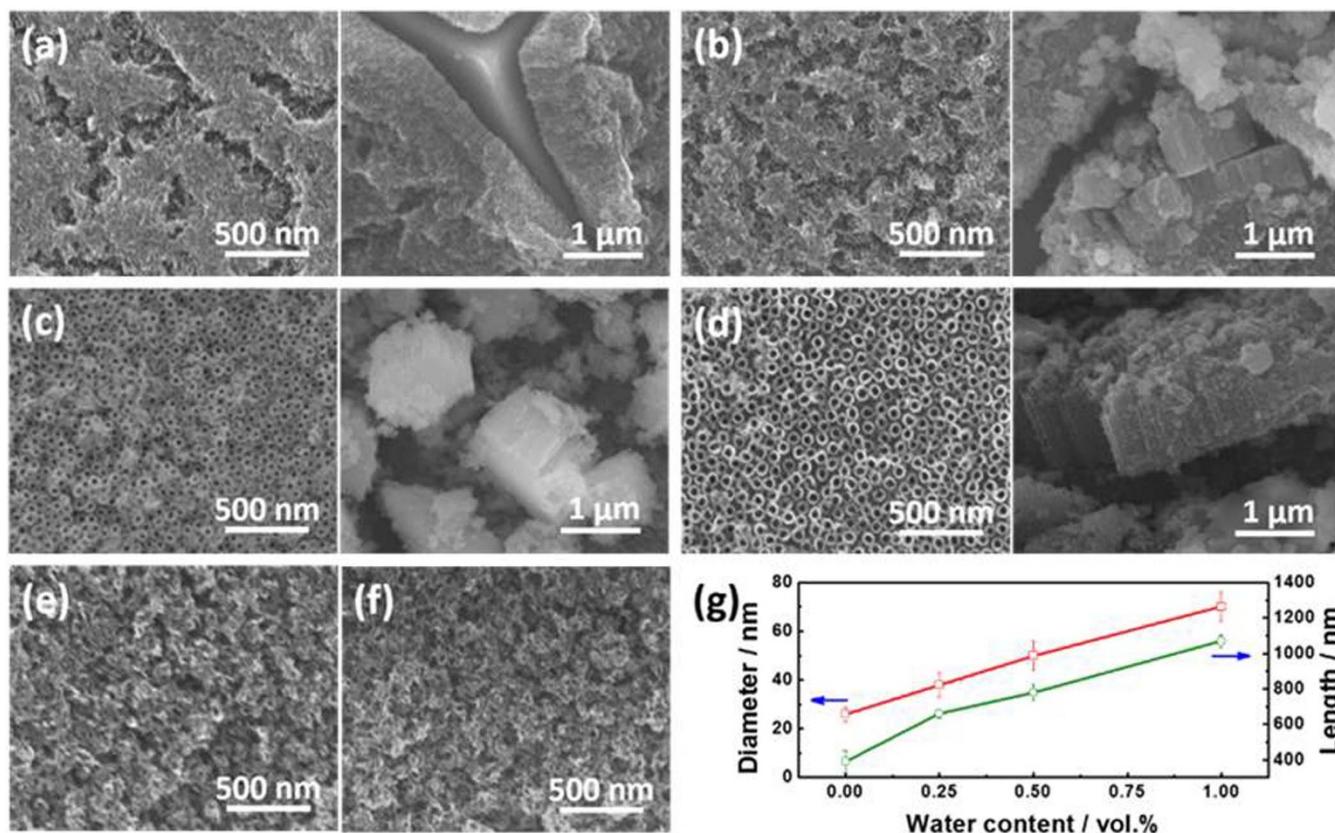
Figure 4 | Surface and cross-sectional FE-SEM images of the Ni-Ti-O NTAs formed at 25 V and 30°C for 1 h in ethylene glycol with 0.2 wt% NH₄F and different H₂O contents. (a) 0.0 vol%, (b) 0.25 vol%, (c) 0.5 vol%, (d) 1.0 vol%, (e) 1.5 vol%, and (f) 2.0 vol%. Variation in the diameter and length of the NTs as a function of H₂O content (g).

H₂O content. Since the F^- ion concentration in the electrolyte is constant, the etching rate of the NT bottom is the same. As a result of the electric field, H_2O in the electrolyte is deprotonated to generate H^+, O^{2-}, and/or OH^- and anions migrate to the oxide/metal interface forming the oxide. As the H_2O content goes up, the availability of anions at the oxide/metal interface increases and consequently the oxide growth rate as well. The NT bottom thickness is proportional to the NT diameter[3] and so a linear relationship between the electrolyte H_2O content and NT diameter is observed. By the same token, the constant chemical etching rate of F^- of the top of NTs and fast growth of NTs at a larger H_2O concentration increase the NT length. Micropit formation and current fluctuations are observed when the H_2O content is less than 0.5 vol% (Figure S8 and S4c), but the morphology of the micropits is different from that shown in Figures S1 and S7 indicative of different formation mechanisms.

The presence of F^- in the electrolyte is essential to the formation of NTAs[3]. The major effect is to etch the bottom of the NTs at a proper rate to maintain a relatively constant bottom oxide thickness. The F^- concentration has a significant influence on the NT diameter and length as illustrated in Figure 5. The samples are anodized at 30°C and 25 V in ethylene glycol with 1.0 vol% H_2O and different NH_4F contents for 1 h. As the NH_4F concentration is increased from 0.025 wt% to 1.0 wt%, the NT diameter increases from 33 nm to a maximum of 70 nm for 0.2 wt% NH_4F and then diminishes gradually to 39 nm for 0.8 wt% NH_4F. The variation in the NT length exhibits the same tendency as the NT diameter. Excess F^- leads to rapid dissolution of the oxide thus hampering the ability to generate the regular nanotubular structure (Figure 5g). The variations in the Ni-Ti-O NT diameter and length is the same as those of the TiO_2 NTs[29]. One possible explanation is that a small F^- concentration reduces the growth rate of the NTs and prolongs the attack by H^+

produced by H_2O deprotonation of the NT bottom. In comparison, a high F^- concentration expedites the anodization process thus reducing the impact of H^+ etching and increasing the NT diameter. However, too much F^- in the electrolyte accelerates electrochemical etching of the NT bottom and chemical dissolution of the NT top thus decreasing the NT diameter and length. It is noted that corrosion micropits can occasionally be observed from the samples when the NH_4F concentration is small (Figure S9).

By modulating the various anodization parameters discussed above, precise structural control of the Ni-Ti-O TNAs can be accomplished. In order to better understand the microstructure of the NTAs, HR-TEM inspection is conducted (Figure S10). The low magnification TEM image (Figure S10(a)) shows the length and diameter of the NTs, being consistent with that observed by FE-SEM. The HR-TEM image and SAED pattern (Figure S10(b)) display the amorphous structure of the NTs. The EDS line scanning of Ni, Ti and O along the longitudinal direction of the NTs (Figure S10(c)) displays that the ratio Ni to Ti is lower at the top area of the NTAs compared to that at the bottom area, indicating that the Ni oxide dissolves preferentially compared to the Ti oxide during anodization.

The potential applications of NTAs to energy, biomedical and environment fields are subsequently explored. One potential application of the Ni-Ti-O NTAs is the electrode in electrochemical energy storage and the preparation parameters and morphology of the NTAs are presented in Figure S11. Figure 6 displays the electrochemical characterization results. A pair of distinct anodic and cathodic peaks with a symmetrical structure is observed from the cyclic voltammetry (CV) curves (Figure 6a) and the intensity increases with the scanning rate, implying good reversibility in the faradic oxidation and reduction reactions at the interface between the NTAs and electrolyte. The XPS results of the Ni-Ti-O NTAs in Figure S12 have
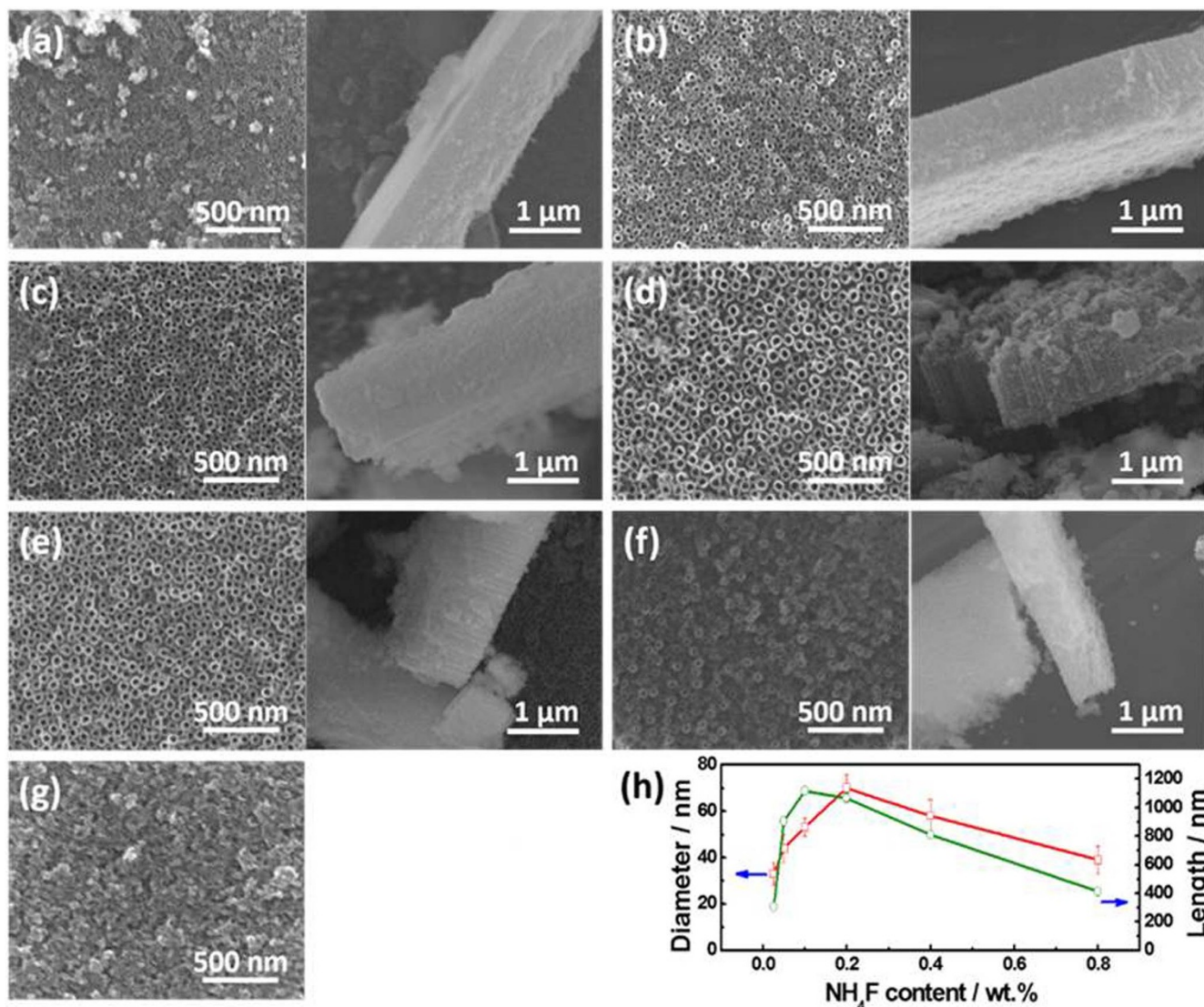
Figure 5 | Surface and cross-sectional FE-SEM images of the Ni-Ti-O NTAs formed at 25 V and 30°C for 1 h in ethylene glycol solution with 1.0 vol% H$_2$O and different NH$_4$F concentrations. (a) 0.025 wt%, (b) 0.05 wt%, (c) 0.1 wt%, (d) 0.2 wt%, (e) 0.4 wt%, (f) 0.8 wt%, and (g) 1.0 wt%. Variation in the diameter and length of the NTs as a function of NH$_4$F concentration (h).

shown that the Ni2p1/2 and Ni2p3/2 is centered at 856.0 and 873.6 eV, respectively, with a spin-energy separation of 17.6 eV, which well matches the characteristic of Ni(OH)$_2$ as previously reported[31]. Based on our XPS results and previous report[32], the two peaks can be attributed to the conversion between the different oxidation states of Ni according to the follow reaction:

$$Ni(OH)_2 + OH^- \leftrightarrow NiOOH + H_2O + e^- \qquad (1)$$

The variation in the capacitance versus scanning rate derived from the CV curves in Figure 6a is displayed in Figure 6b which shows relatively rapid charging/discharging kinetics. As shown in the galvanostatic charge-discharge (GCD) voltage profiles in Figure 6c, a Columbic efficiency of nearly 100% can be observed from each cycle at a current density of 0.4 mA/cm^2. The good cycling stability of the Ni-Ti-O NTAs is demonstrated in Figure 6d. The capacitance increases by about 9% during the first 100 cycles and it may be attributed to the activation process of the electrodes. Remarkably, the capacitance only decreases by only 3.2% after the 1000-cycle test. Nearly twice the capacitance is observed from the Ni-Ti-O NTAs at a current density of 0.4 mA/cm^2 compared to previous work[19]. It is

well known that high electrical conductivity of the electrode will contribute to the capacitance properties. The conducting behavior of the Ni-Ti-O NTAs is investigated by EIS and the Nyquist plot is shown in Figure 6e where the high frequency region of the plot is shown as an inset. Conventional electrode materials usually show a semicircular arc, corresponding to the charge transfer between the electrode and the electrolyte. However, no semicirlce is observed for the Ni-Ti-O NTAs, which indicates the absence of electrical resistance and the potential availability as the supercapacitor electrode. Salari and co-authors ascribe this phenomenon to the greatly improved electron transfer pathways in the highly ordered NTAs compared to disordered structure[33]. The aforementioned results suggest that the Ni-Ti-O NTAs are potential electrode materials in electrochemical energy storage due to fast charging/discharging kinetics and good cycling stability.

In the biomedical fields, an important application of the Ni-Ti-O NTAs is concerned with biofunctional coatings on NiTi-based biomedical implants. The NTAs have been shown to induce selective differentiation of mesenchymal stem cells (MSCs) into osteoblasts[9], enhance osteoblast and endothelial functions[25,34] and reduce adhesion of macrophages[35]. Hence, the biofunctionality of NiTi alloy is expected to be enhanced by forming the NTAs coating on the surface.
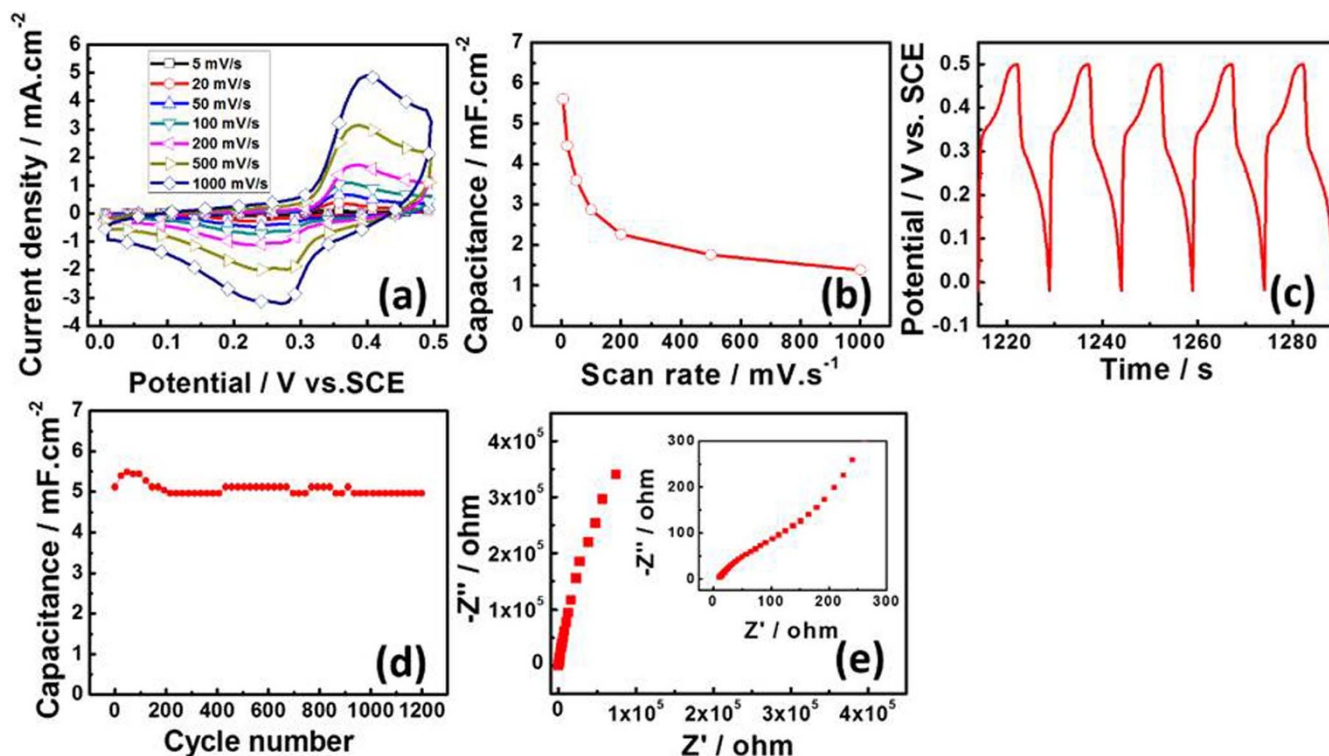
Figure 6 | Electrochemical characterization of the Ni-Ti-O NTAs. (a) CV curves acquired at various scanning rates. (b) Capacitance obtained at various scanning rates. (c) GCD voltage profiles obtained at a current density of 0.4 mA/cm². (d) Cycling performance at a current density of 0.4 mA/cm². (e) Nyquist plot of the Ni-Ti-O NTAs.

The preparation parameters and morphology of the NTAs used in biological experiments are presented in Figure S13. As shown by the live/dead staining results in Figure 7, the NTAs support cell growth similar to the control. In addition, the tubular structure of the NTAs serves as a good carrier for delivery of drugs and species such as growth factors[36], antibiotics[37] as well as inorganic biofunctional elements[8,13,38] to cater to different clinical requirements. Another potential application for the Ni-Ti-O NTAs in the biomedical fields is as the electrode of non-enzymatic glucose sensor. Ni has been recognized to be able to direct the electrooxidation of glucose to glucolac-

tone through the redox reaction of equation (1) and the following equation[39]:

$$NiOOH + glucose \rightarrow Ni(OH)_2 + glucolactone \qquad (2)$$
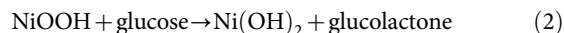
This electrochemical process is a kinetically controlled surface reaction, so the NTAs with large specific area can provide more active sites. As shown in Figure 8, the amperometric response of the Ni-Ti-O NTAs is ten times of that of the mirror polished NiTi alloy, indicating their significantly enhanced electrooxidation of glucose.

TiO_2 is an n-type semiconductor and NiO is a p-type semiconductor. It has been reported that the p-n junction can enhance the photocatalytic activity of TiO_2 by retarding electron-hole recombination[40]. The Ni-Ti-O NTAs are promising materials in the energy field, for example, evolution of hydrogen[21] and conversion of solar energy[41]. Nonetheless, our data show that the Ni-Ti-O NTAs have poor photocatalytic activity (Figure S14). One possible explanation is that the Ni content in the Ni-Ti-O NTAs is too high thus blocking the active site in TiO_2. Systemic research concerning the photocatalytic activity of the NTAs is in progress and additional findings will be reported in due course.

Different applications may require Ni-Ti-O NTAs with specific diameter and length. For example, in order to promote adhesion and proliferation and inhibit differentiation of MSCs, NTs with a small diameter is required, while large NTs may induce selective differentiation of the MSCs into osteoblast cells[42]. NiO is inexpensive and desirable in gas sensors, resistance switches, and electrochromic devices. In most of the applications, the specific surface area needs to be maximized to improve the efficiency. Our results demonstrate that by varying the processing parameters, the diameter, length, and composition (Figure S12) of the Ni-Ti-O NTAs can be tailored to meet the various requirements to widen the use of the materials in the different fields.
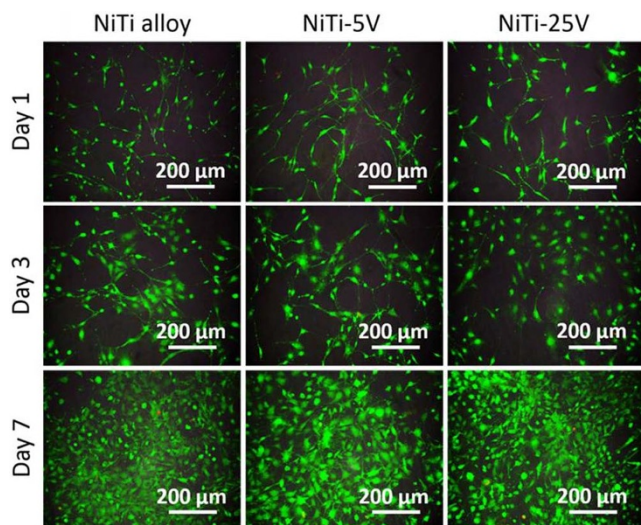

Figure 7 | Fluorescence images of Live/dead staining of MC3T3-E1 cells after culturing for 1, 3 and 7 days on the the Ni-Ti-O NTAs and NiTi alloy control.
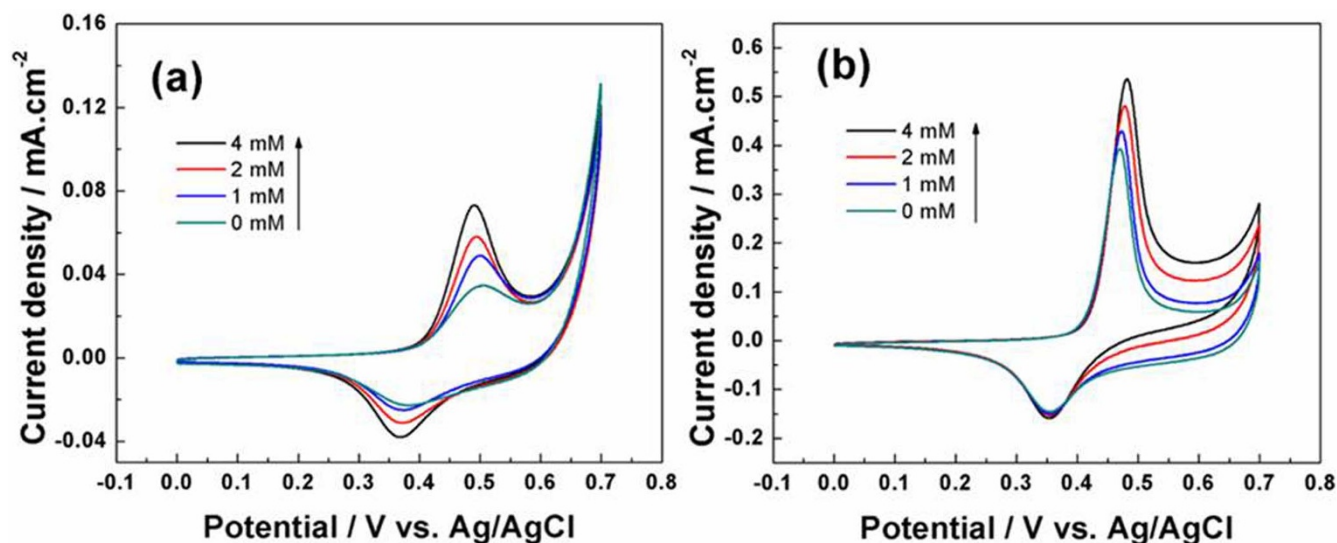
7

Figure 8 | CVs of the NiTi alloy (a) and Ni-Ti-O NTs (b) in 0.1 M NaOH with different glucose concentrations at a scanning rate of 50 mV/s. All samples were activated at 50 mV/s for 100 cycles.

Conclusions

In summary, the diameter and length of the Ni-Ti-O NTAs can be tailored in a controlled manner despite the large fraction of Ni in NiTi alloys. To form well-defined NTs, the anodization voltage, temperature, and NH_4F concentration in the electrolyte can be varied in a relatively wide range but the optimal concentration range of H_2O in the electrolyte is narrower. By adjusting these conditions, the Ni-Ti-O NTAs with different diameters (15–70 nm) and lengths (45–1320 nm) can been fabricated. The results also provide insights into the anodization of other Ti alloys containing a large fraction of non-valve metals. The Ni-Ti-O NTAs show promising potential in the energy and biomedical fields.

1. Mor, G. K., Shankar, K., Paulose, M., Varghese, O. K. & Grimes, C. A. Use of highly-ordered TiO₂ nanotube arrays in dye-sensitized solar cells. *Nano lett.* **6**, 215–218 (2006).
2. Park, J. H., Kim, S. & Bard, A. J. Novel carbon-doped TiO₂ nanotube arrays with high aspect ratios for efficient solar water splitting. *Nano lett.* **6**, 24–28 (2006).
3. Roy, P., Berger, S. & Schmuki, P. TiO₂ nanotubes: synthesis and applications. *Angew. Chem. Int. Edit.* **50**, 2904–2939 (2011).
4. Macak, J. M., Zlamal, M., Krysa, J. & Schmuki, P. Self-organized TiO₂ nanotube layers as highly efficient photocatalysts. *Small* **3**, 300–304 (2007).
5. Albu, S. P., Ghicov, A., Macak, J. M., Hahn, R. & Schmuki, P. Self-organized, free-standing TiO₂ nanotube membrane for flow-through photocatalytic applications. *Nano lett.* **7**, 1286–1289 (2007).
6. Park, J., Bauer, S., von der Mark, K. & Schmuki, P. Nanosize and vitality: TiO₂ nanotube diameter directs cell fate. *Nano lett.* **7**, 1686–1691 (2007).
7. Song, Y.-Y., Schmidt-Stein, F., Bauer, S. & Schmuki, P. Amphiphilic TiO₂ nanotube arrays: an actively controllable drug delivery system. *J. Am. Chem. Soc.* **131**, 4230–4232 (2009).
8. Zhao, L. *et al.* Antibacterial Nano-structured titania coating incorporated with silver nanoparticles. *Biomaterials* **32**, 5706–5716 (2011).
9. Zhao, L., Liu, L., Wu, Z., Zhang, Y. & Chu, P. K. Effects of micropitted/nanotubular titania topographies on bone mesenchymal stem cell osteogenic differentiation. *Biomaterials* **33**, 2629–2641 (2012).
10. Regonini, D., Bowen, C., Jaroenworaluck, A. & Stevens, R. A review of growth mechanism, structure and crystallinity of anodized TiO₂ nanotubes. *Mater. Sci. Eng.: R* **74**, 377–406 (2013).
11. Lee, K., Hahn, R., Altomare, M., Selli, E. & Schmuki, P. Intrinsic Au decoration of growing TiO₂ nanotubes and formation of a high-efficiency photocatalyst for H₂ production. *Adv. Mater.* **25**, 6133–6137 (2013).
12. Hang, R. *et al.* Antibacterial activity and cytocompatibility of Cu–Ti–O nanotubes. *J. Biomed. Mater. Rese. Part A* **102**, 1850–1858 (2014).
13. Gao, A. *et al.* The effects of titania nanotubes with embedded silver oxide nanoparticles on bacteria and osteoblasts. *Biomaterials* **35**, 4223–4235 (2014).
14. Mor, G. K., Prakasam, H. E., Varghese, O. K., Shankar, K. & Grimes, C. A. Vertically oriented Ti-Fe-O nanotube array films: toward a useful material architecture for solar spectrum water photoelectrolysis. *Nano lett.* **7**, 2356–2364 (2007).
15. Mohapatra, S. K., Raja, K. S., Misra, M., Mahajan, V. K. & Ahmadian, M. Synthesis of self-organized mixed oxide nanotubes by sonoelectrochemical anodization of Ti–8Mn alloy. *Electrochim. Acta* **53**, 590–597 (2007).
16. Roy, P. *et al.* Oxide nanotubes on Ti-Ru alloys: strongly enhanced and stable photoelectrochemical activity for water splitting. *J. Am. Chem. Soc.* **133**, 5629–5631 (2011).
17. Jeong, Y.-H., Lee, K., Choe, H.-C., Ko, Y.-M. & Brantley, W. A. Nanotube formation and morphology change of Ti alloys containing Hf for dental materials use. *Thin Solid Films* **517**, 5365–5369 (2009).
18. Yang, Y., Kim, D., Yang, M. & Schmuki, P. Vertically aligned mixed V₂O₅–TiO₂ nanotube arrays for supercapacitor applications. *Chem. Commun.* **47**, 7746–7748 (2011).
19. Kim, J.-H., Zhu, K., Yan, Y., Perkins, C. L. & Frank, A. J. Microstructure and pseudocapacitive properties of electrodes constructed of oriented NiO-TiO₂ nanotube arrays. *Nano lett.* **10**, 4099–4104 (2010).
20. Minagar, S., Berndt, C. C., Gengenbach, T. & Wen, C. Fabrication and characterization of TiO₂-ZrO₂–ZrTiO₄ nanotubes on TiZr alloy manufactured via anodization. *J. Mater. Chem. B* **2**, 71–83 (2014).
21. Sreethawong, T., Suzuki, Y. & Yoshikawa, S. Photocatalytic evolution of hydrogen over mesoporous TiO₂ supported NiO photocatalyst prepared by single-step Sol–Gel process with surfactant template. *Int. J. Hydrogen Energy* **30**, 1053–1062 (2005).
22. Hoa, N. D. & El-Safty, S. A. Synthesis of mesoporous NiO nanosheets for the detection of toxic NO₂ gas. *Chem.-Eur. J.* **17**, 12896–12901 (2011).
23. He, L. *et al.* Memory and threshold resistance switching in Ni/NiO core–shell nanowires. *Nano lett.* **11**, 4601–4606 (2011).
24. Moulki, H. *et al.* Improved electrochromic performances of NiO based thin films by lithium addition: from single layers to devices. *Electrochim. Acta* **74**, 46–52 (2012).
25. Zhao, L., Mei, S., Chu, P. K., Zhang, Y. & Wu, Z. The influence of hierarchical hybrid micro/nano-textured titanium surface with titania nanotubes on osteoblast functions. *Biomaterials* **31**, 5072–5082 (2010).
26. Hang, R., Huang, X., Tian, L., He, Z. & Tang, B. Preparation, characterization, corrosion behavior and bioactivity of Ni₂O₃-doped TiO₂ nanotubes on NiTi alloy. *Electrochim. Acta* **70**, 382–393 (2012).
27. Qin, R. *et al.* Ni-doped TiO₂ nanotube arrays on shape memory alloy. *Appl. Surf. Sci.* **257**, 6308–6313 (2011).
28. Huan, Z., Fratila-Apachitei, L., Apachitei, I. & Duszczyk, J. Synthesis and characterization of hybrid micro/nano-structured NiTi surfaces by a combination of etching and anodizing. *Nanotechnology* **25**, 055602 (2014).
29. Wang, D., Liu, Y., Yu, B., Zhou, F. & Liu, W. TiO₂ nanotubes with tunable morphology, diameter, and length: synthesis and photo-electrical/catalytic performance. *Chem. Mater.* **21**, 1198–1206 (2009).
30. Crawford, G. & Chawla, N. Porous hierarchical TiO₂ nanostructures: processing and microstructure relationships. *Acta Mater.* **57**, 854–867 (2009).
31. Yan, J. *et al.* Advanced asymmetric supercapacitors based on Ni(OH)₂/graphene and porous graphene electrodes with high energy density. *Adv. Func. Mater.* **22**, 2632–2641 (2012).
32. Yang, S. *et al.* Spherical α-Ni (OH)₂ nanoarchitecture grown on graphene as advanced electrochemical pseudocapacitor materials. *Chem. Commun.* **48**, 2773–2775 (2012).
33. Salari, M., Aboutalebi, S. H., Konstantinov, K. & Liu, H. K. A highly ordered titania nanotube array as a supercapacitor electrode. *Phys. Chem. Chem. Phys.* **13**, 5038–5041 (2011).

34. Peng, L., Eltgroth, M. L., LaTempa, T. J., Grimes, C. A. & Desai, T. A. The effect of TiO₂ nanotubes on endothelial function and smooth muscle proliferation. *Biomaterials* **30**, 1268–1272 (2009).

35. Rajyalakshmi, A., Ercan, B., Balasubramanian, K. & Webster, T. J. Reduced adhesion of macrophages on anodized titanium with select nanotube surface features. *Int. J. Nanomed.* **6**, 1765–1771 (2011).

36. Park, J. *et al.* Synergistic control of mesenchymal stem cell differentiation by nanoscale surface geometry and immobilized growth factors on TiO₂ nanotubes. *Small* **8**, 98–107 (2012).

37. Popat, K. C., Eltgroth, M., LaTempa, T. J., Grimes, C. A. & Desai, T. A. Decreased *Staphylococcus epidermis* adhesion and increased osteoblast functionality on antibiotic-loaded titania nanotubes. *Biomaterials* **28**, 4880–4888 (2007).

38. Zhao, L. *et al.* The osteogenic activity of strontium loaded titania nanotube arrays on titanium substrates. *Biomaterials* **34**, 19–29 (2013).

39. Gao, Z. D., Han, Y., Wang, Y., Xu, J. & Song, Y. Y. One-step to prepare self-organized nanoporous NiO/TiO₂ layers and its use in non-enzymatic glucose sensing. *Sci. Rep.* **3**, 3323 (2013).

40. Yu, J., Wang, W. & Cheng, B. Synthesis and enhanced photocatalytic activity of a hierarchical porous flowerlike p—n junction NiO/TiO₂ photocatalyst. *Chem.-Asian J.* **5**, 2499–2506 (2010).

41. Irwin, M. D., Buchholz, D. B., Hains, A. W., Chang, R. P. & Marks, T. J. P-type semiconducting nickel oxide as an efficiency-enhancing anode interfacial layer in polymer bulk-heterojunction solar cells. *Proc. Natl. Acad. Sci. U S A* **105**, 2783–2787 (2008).

42. Oh, S. *et al.* Stem cell fate dictated solely by altered nanotube dimension. *Proc. Natl. Acad. Sci. U S A* **106**, 2130–2135 (2009).

Acknowledgments

Author contributions

Y.L., A.G. and L.B. prepared and characterized the anodized samples. X.H., X.Z. and B.T. carried out the performance measurements. R.H. designed the experiments and wrote the main manuscript text. L.Z. designed the experiments with R.H. and revised the manuscript. P.K.C. advised and revised the manuscript. All authors reviewed the manuscript.

Additional information

Supplementary information accompanies this paper at http://www.nature.com/scientificreports

Competing financial interests: The authors declare no competing financial interests.

How to cite this article: Hang, R. *et al.* Fabrication of Ni-Ti-O nanotube arrays by anodization of NiTi alloy and their potential applications. *Sci. Rep.* **4**, 7547; DOI:10.1038/srep07547 (2014).